

Turbulent Proton Heating Rate in the Solar Wind from 5 to 45 R_{\odot}

K. SASIKUMAR RAJA,^{1,2} PRASAD SUBRAMANIAN,³ MADHUSUDAN INGALE,³ R. RAMESH,² AND
MILAN MAKSIMOVIC¹

¹*LESIA, Observatoire de Paris, Université PSL, CNRS, Sorbonne Université, Université de Paris, 5 place Jules
Janssen, 92195 Meudon, France.*

²*Indian Institute of Astrophysics, 2nd Block, Koramangala, Bangalore - 560 034, India.*

³*Indian Institute of Science Education and Research, Pashan, Pune - 411 008, India.*

ABSTRACT

Various remote sensing observations have been used so far to probe the turbulent properties of the solar wind. Using the recently reported density modulation indices that are derived using angular broadening observations of Crab Nebula during 1952 - 2013, we measured the solar wind proton heating using the kinetic Alfvén wave dispersion equation. The estimated heating rates vary from $\approx 1.58 \times 10^{-14}$ to 1.01×10^{-8} erg cm⁻³ s⁻¹ in the heliocentric distance range 5 - 45 R_{\odot} . Further, we found that heating rates vary with the solar cycle in correlation with density modulation indices. The models derived using in-situ measurements (for example, electron/proton density, temperature, and magnetic field) that the recently launched Parker Solar Probe observes (planned closest perihelia 9.86 R_{\odot} from the center of the Sun) are useful in the estimation of the turbulent heating rate precisely. Further, we compared our heating rate estimates with the one derived using previously reported

remote sensing and in-situ observations.

Keywords: occultations - scattering - solar wind - Sun: corona - Sun: radio radiation - turbulence

1. INTRODUCTION

Even after decades of intense research, we do not know the precise solar wind heating mechanism and its acceleration. The in-situ observations confirm that solar wind undergoes extended non-adiabatic heating (Freeman 1988; Gazis et al. 1994; Matthaeus et al. 1999; Richardson & Smith 2003). More details on turbulent heating and solar wind acceleration are given by Cranmer et al. (2007); Chandran & Hollweg (2009b); Verdini et al. (2010); Cranmer et al. (2013); Woolsey & Cranmer (2014); Zank et al. (2018). Interaction between counter-propagating Alfvén waves causes the wave energy to cascade into small scales. When the scale sizes which are perpendicular to the background magnetic field direction (λ_{\perp}) are comparable to the proton gyroradius (ρ_p), the wave energy begin to dissipate and thereby heats the plasma. It is known that when $\lambda_{\perp} \gg l_i = v_A/\Omega_p$, (where l_i is the proton inertial length, v_A is the Alfvén speed and Ω_p is the proton cyclotron frequency) the Alfvén waves are non-compressive. But there is a considerable evidence that when the scale sizes are in the range $\rho_p \lesssim \lambda_{\perp} \lesssim l_i$, they are compressive (e.g., Harmon 1989; Hollweg 1999; Chandran et al. 2009a). Also, the waves become dispersive and damp for the scales $\lambda_{\perp} \lesssim \rho_p$.

In order to estimate the heating rates in the solar wind, we used the recently reported density modulation indices ($\epsilon_N = \delta_N/N$, where δ_N is the rms density fluctuations and ‘N’ is the ambient background density) derived using the Crab Nebula occultation observations carried out during 1952 - 2013 (Machin & Smith 1952; Slee 1959; Hewish & Wyndham 1963; Erickson 1964; Blesing & Dennison 1972; Dennison & Blesing 1972; Sastry & Subramanian 1974; Armstrong et al. 1990; Anantharamaiah et al. 1994; Subramanian 2000; Ramesh et al. 2001; Sasikumar Raja et al. 2016, 2017, 2019a). In this technique, when a radio point source (in this study Crab Nebula), observed through the foreground solar wind (in June of every year), we can have the following obser-

vations: (i) the radio source’s angular broadening increases due to the turbulent medium’s scattering, (ii) since we observe the radio sources whose flux density is constant over a long time, the peak flux density decreases as the source size increases; but the integrated flux density remains constant, (iii) the radio sources broaden anisotropically for the heliocentric distance below $10 R_{\odot}$, and thus we can measure the parameter anisotropy (i.e., the ratio between the major to the minor axis of radio source) (Blesing & Dennison 1972; Dennison & Blesing 1972; Sasikumar Raja et al. 2017), and (iv) position angle of the major axis of the source (measured from the north through the east). Having such observations, Sasikumar Raja et al. (2016) have derived the density modulation indices in the heliocentric distance 5 - 45 R_{\odot} . In this article, we use those density modulation indices to measure the proton heating rate (ϵ_{k_i}) by making use of kinetic Alfvén wave dispersion equations (see §3.4) and compared the results with the recent reports that are measured using angular broadening (Sasikumar Raja et al. 2017) and interplanetary scintillation observations (Bisoi et al. 2014; Ingale 2015b). We also compare our results with the recently reported heating rates derived using the in-situ observations of Adhikari et al. (2020) and Bandyopadhyay et al. (2020). Further, we report the way heating rates vary with the heliocentric distance and the way it vary with the solar cycle.

2. OBSERVATIONS

The angular broadening of the Crab Nebula is first observed by Machin & Smith (1952). Since then, many authors have reported similar observations as previously mentioned (see §1). In this article, we present results derived using data obtained by the Gauribidanur radioheliograph (GRAPH) during 2011 - 2013 (Ramesh et al. 1998; Ramesh 2011, 2014) and other historical observations carried out during 1952 - 1963 (Machin & Smith 1952; Hewish 1957, 1958; Hewish & Wyndham 1963; Sasikumar Raja et al. 2016). For instance, Figure 1 shows the observation of GRAPH carried out at 80 MHz over an interferometer baseline of 1600 meters. The top panel shows the schematic of the Crab Nebula occultation technique. The red and green circles indicate the sun and location of the Crab Nebula on different days of June in 2011 and 2013. The bottom panel shows the decrement in flux density as the Crab Nebula ingresses and becomes invisible during 12 - 18 June and then increments as it egresses. The flux density during 2013 is lower (compared to 2011) as it corresponds

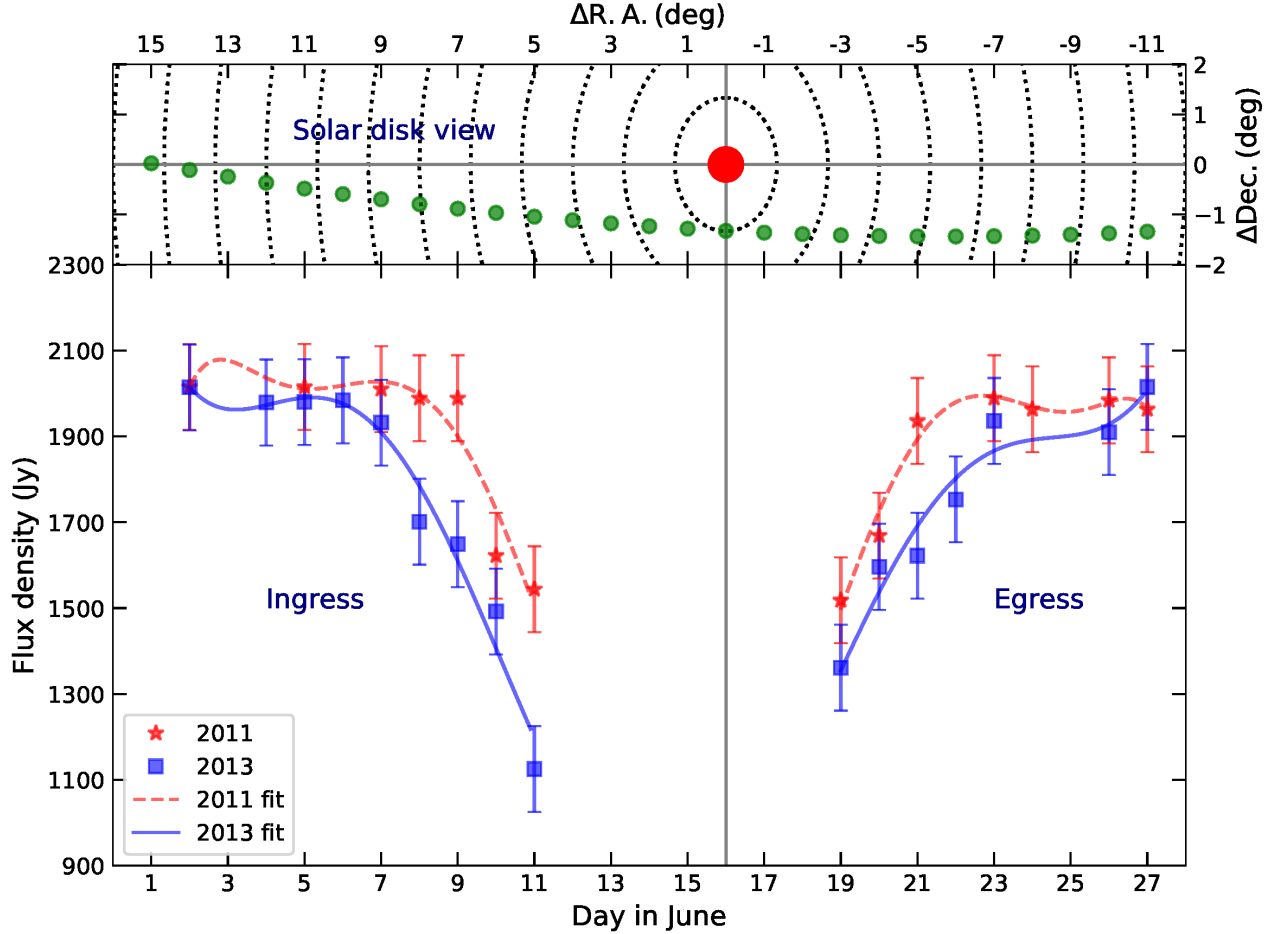


Figure 1. (top) Solar disk view of the Crab Nebula occultation. The red circle indicates the Sun and green circles represent the location of Crab Nebula with respect to the Sun in different days of June. $\Delta R.A.$ and $\Delta Dec.$ are the offset distances of Crab Nebula from the Sun in right ascension and declination, respectively. The closest dotted concentric circle around the Sun has a radius of $5 R_{\odot}$ and the radii of the rest of the circles differ from their adjacent ones by $5 R_{\odot}$. (bottom) The observed flux densities of the Crab Nebula on different days during its occultation by the solar corona. The periods before and after June 16th correspond to the ingress and egress, respectively. The markers ‘*’ and ‘square’ indicate the observations carried out in June 2011 and June 2013, respectively. The minimum detectable flux density of the GRAPH ≈ 100 Jy is used as the error associated with these measurements.

to the solar maximum. We make a note that the latter observations are carried out over interferometer baselines in the range 60 - 1000 meters and the frequency range 26-158 MHz. Therefore, Sasikumar Raja et al. (2016) have scaled these structure functions to the largest baseline of GRAPH (1600 meters; before the extension) and its routinely observed frequency 80 MHz using the gen-

eral structure-function (see §3). For the sake of completeness, we summarize a method using which Sasikumar Raja et al. (2016) have derived the density modulation indices (see Figure 2) and the way we have measured proton heating rate in the following sections.

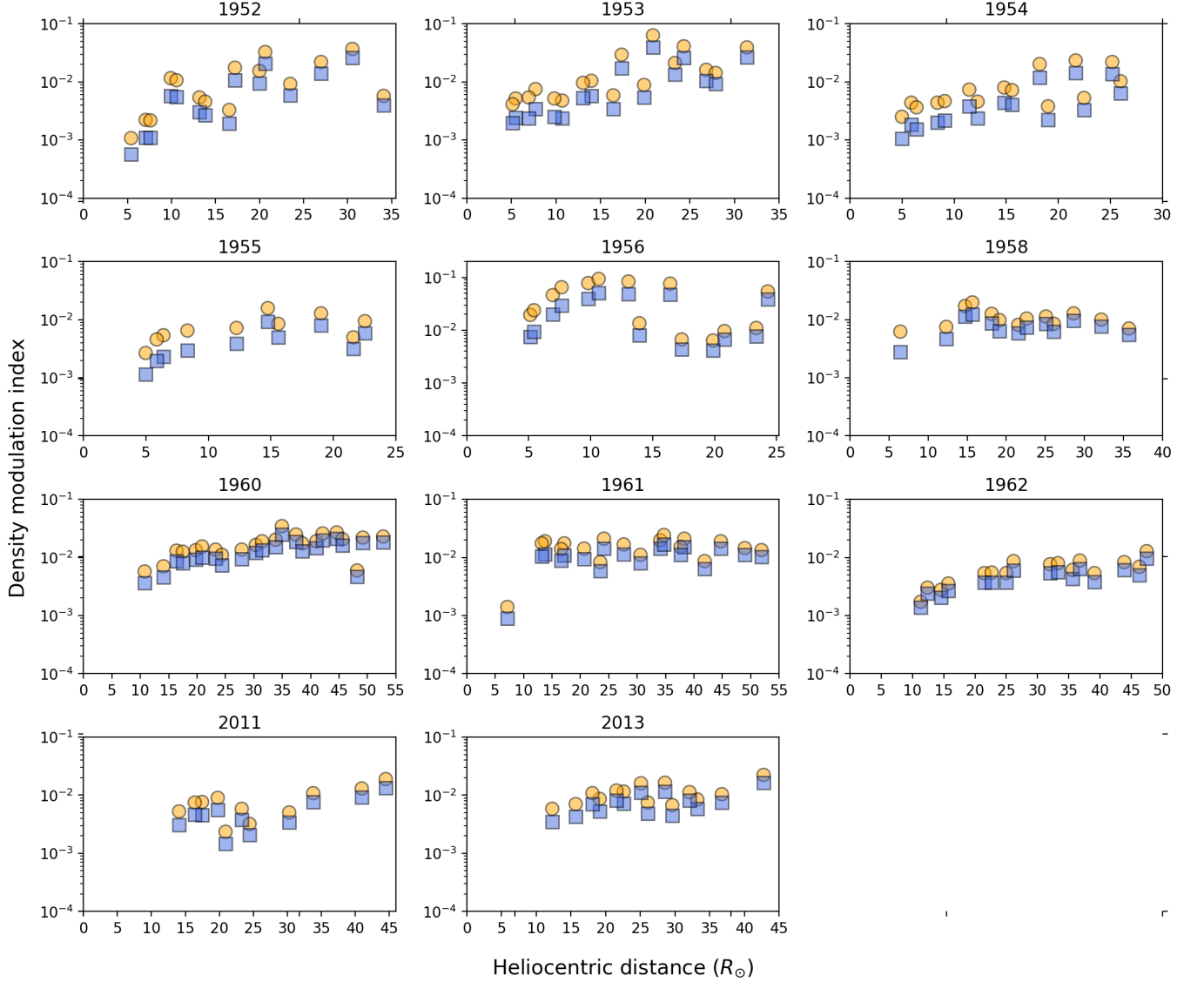


Figure 2. Heliocentric dependence of the density modulation index in different years. The markers ‘circle’ and ‘square’ indicate modulation indices that are derived using the proton inertial length and proton gyroradius model, respectively.

3. RESULTS AND DISCUSSIONS

In the solar wind, turbulent density inhomogeneities play a vital role in scattering of the radio waves (Coles & Harmon 1989; Yamauchi et al. 1998; Bisoi et al. 2014; Mugundhan et al. 2017; Krupar et al. 2018; Sasikumar Raja et al. 2019b; Krupar et al. 2020). Such inhomogeneities are represented by a spatial power spectrum. It comprises a power-law together with an exponential turnover at the inner scale. In the case of isotropic medium, the turbulent spatial power spectrum ($P_{\delta N}$) is defined as (Bastian 1994; Ingale et al. 2015a),

$$P_{\delta N}(k, R) = C_N^2(R)k^{-\alpha} \times \exp -(kl_i(R)/2\pi)^2, \quad (1)$$

where k is the wavenumber, l_i is the inner/ dissipation scale, and C_N^2 is the amplitude of density turbulence. It is worth mentioning that the injected large-scale energy in the solar wind breaks up into smaller scales until it is dissipated by heating the protons via gyro-resonant interactions. Also, we make a note that the scales at which the energy is injected are called ‘outer scales’, and the scales at which the dissipation happens are called ‘inner scales’ (Kulsrud 2005). Using remote sensing observations, it is found that, at large scales, the density spectrum follows the Kolmogorov scaling law with $\alpha = 11/3$ (Coles & Harmon 1989; Spangler 2002). However, at small scales, the spectrum flattens to $\alpha = 3$ (Coles & Harmon 1989). In this article, since we are interested in the density fluctuations and proton heating rate near the dissipation scales, we have used $\alpha = 3$. We make a note here that C_N^2 are measured for both proton inertial scale model (Coles & Harmon 1989; Leamon et al. 1999, 2000; Smith et al. 2001; Chen et al. 2014a; Bruno & Trenchi 2014; Sasikumar Raja et al. 2019a) and proton gyroradius model (Bale et al. 2005; Sahraoui et al. 2013; Bisoi et al. 2014; Chen et al. 2014b; Sasikumar Raja et al. 2019a). Note that Sasikumar Raja et al. (2016) measured the C_N^2 for two cases of proton temperatures $T_i = 10^5$ K and $T_i = 10^6$ K.

3.1. Measurement of phase structure function

A plane wave from a distant radio point source observed through the solar wind experiences loss of spatial and temporal coherence due to the refraction and scattering caused by the density inhomogeneities. The spatial coherence of the plane wave observed through the scattering medium (i.e.,

solar wind) is described by the mutual coherence function ($\Gamma(s)$), which is in turn related to the phase structure function ($D_\phi(s)$). We make a note that $D_\phi(s)$ provides the information to the extent to which ideal point source is broadened and it contains information about the spectrum of density turbulence. In general, the phase structure function is defined as (Coles & Harmon 1989; Bastian 1994; Ingale et al. 2015a),

$$D_\phi(s) = \langle [\phi(r) - \phi(r + s)]^2 \rangle, \quad (2)$$

where, $\langle \rangle$ indicates the time average, ‘s’ is the baseline of an interferometer, and $\phi(r)$ and $\phi(r + s)$ are the geometric phase delays in the line-of-sight direction through a turbulent medium at positions r and $r + s$.

Using the Crab Nebula occultation observations we measure ($\Gamma(s)$) using,

$$\Gamma(s) = \frac{V(s)}{V(0)}, \quad (3)$$

where, $V(s)$ is the peak flux density of the Crab Nebula observed through the scattering medium over a baseline ‘s’, and $V(0)$ is the flux density over a “zero-length” baseline. The quantity $V(0)$ is measured when the Crab Nebula is far from the solar disk and is unresolved; $V(0) \approx 2015$ Jy at 80 MHz (Braude et al. 1970; McLean & Labrum 1985; Sasikumar Raja et al. 2017).

By knowing the $\Gamma(s)$, we measured the density structure function ($D_\phi(s)$) using (Prokhorov et al. 1975; Ishimaru 1978; Coles & Harmon 1989; Armstrong et al. 1990),

$$D_\phi(s) = -2\ln\Gamma(s) = -2\ln[V(s)/V(0)]. \quad (4)$$

3.2. The amplitude of density turbulence spectrum (C_N^2)

By knowing the structure functions, we measured the amplitude of the turbulence (C_N^2) using the General Structure Function (GSF) (Ingale et al. 2015a; Sasikumar Raja et al. 2016, 2017). The GSF is defined as follows,

$$D_\phi(s) = \frac{8\pi^2 r_e^2 \lambda^2 \Delta L}{\rho 2^{\alpha-2} (\alpha-2)} \Gamma\left(1 - \frac{\alpha-2}{2}\right) \frac{C_N^2(R) l_i^{\alpha-2}(R)}{(1 - f_p^2(R)/f^2)} \\ \times \left\{ {}_1F_1\left[-\frac{\alpha-2}{2}, 1, -\left(\frac{s}{l_i(R)}\right)^2\right] - 1 \right\} \text{ rad}^2, \quad (5)$$

where ${}_1F_1$ is the confluent hyper-geometric function, r_e is the classical electron radius, λ is the observing wavelength, R is the heliocentric distance (in units of R_\odot), ΔL is the thickness of the scattering medium ($\approx (\pi/2)R_0$, where R_0 is the impact parameter related to the projected heliocentric distance of the Crab Nebula), f_p and f are the plasma and observing frequencies, respectively and the quantity l_i is the inner scale.

In order to evaluate the inner scales we used the following two prescriptions that are widely used in the literature. The first prescription envisages proton cyclotron damping by Alfvén waves. The inner scales measured using this mechanism are called proton inertial lengths (Coles & Harmon 1989; Leamon et al. 1999, 2000; Smith et al. 2001; Chen et al. 2014a; Bruno & Trenchi 2014; Sasikumar Raja et al. 2019a) which can be written as,

$$l_i(R) = v_A(R)/\Omega_p(R) = 2\pi/k_i(R) = 228/\sqrt{N_e(R)} \text{ km}, \quad (6)$$

where N_e is the electron density in cm^{-3} , k_i is the wavenumber, v_A is the Alfvén speed and Ω_p is the proton gyrofrequency.

The electron density (N_e) is estimated using the Leblanc density model (Leblanc et al. 1998):

$$N_e(R) = 7.2 R^{-2} + 1.95 \times 10^{-3} R^{-4} + 8.1 \times 10^{-7} R^{-6} \text{ cm}^{-3}. \quad (7)$$

where ‘R’ is the heliocentric distance in units of astronomical units (AU, 1 AU = 215 R_\odot).

In the second prescription, the inner scales are measured assuming proton gyroradius model in which dissipation is expected to happen at scales comparable to the proton gyroradius, $\rho_i = V_p/\Omega_p$, where V_p is the proton speed and Ω_p is the proton gyrofrequency (Goldstein et al. 2015). The

proton gyroradius scales are measured using (Bale et al. 2005; Sahraoui et al. 2013; Bisoi et al. 2014; Chen et al. 2014b; Sasikumar Raja et al. 2019a):

$$\rho_i(R) = 1.02 \times 10^2 \mu^{1/2} T_i^{1/2} B(R)^{-1} \text{ cm}, \quad (8)$$

where $\mu (\equiv m_i/m_p)$ is the ion mass (in units of the proton mass), T_i is the proton temperature (in eV) derived using following relations (Venzmer & Bothmer 2018),

$$T_{med}(SSN, R) = (197 \times SSN + 57300) \times R^{-1.10} \text{ K} \quad (9)$$

$$T_{avg}(SSN, R) = 1.654 \times T_{med}(SSN, R), \quad (10)$$

where, T_{med} and T_{avg} are the median and average proton temperatures in K, and SSN is the sunspot number. We make a note that in this article, we have used the revised sunspot number¹ (Clette et al. 2016).

Interplanetary magnetic field (B in Gauss) is measured using the Parker spiral magnetic field model in the ecliptic plane (Williams 1995),

$$B(R) = 3.4 \times 10^{-5} R^{-2} (1 + R^2)^{1/2} \text{ Gauss}. \quad (11)$$

3.3. Estimating the density modulation index ($\epsilon_{N_e} = \delta N_{k_i}/N_e$)

The density fluctuations δN_{k_i} at the inner scale and spatial power spectrum (Equation 1) are related as follows (Chandran et al. 2009a)

$$\delta N_{k_i}^2(R) \sim 4\pi k_i^3 P_{\delta N}(R, k_i) = 4\pi C_N^2(R) k_i^{3-\alpha} e^{-1}, \quad (12)$$

where $k_i \equiv 2\pi/l_i$.

¹ <http://www.sidc.be/silso/datafiles>

By knowing the δN_{k_i} and the background electron density (N_e , § 3.1), the density modulation index (ϵ_{N_e}) can be measured using,

$$\epsilon_{N_e}(R) \equiv \frac{\delta N_{k_i}(R)}{N_e(R)}. \quad (13)$$

For the sake of completeness, the measured density modulation indices and its variation with heliocentric distance is shown in Figure 2 (Sasikumar Raja et al. 2016). Similarly, solar cycle dependence of the density modulation indices is shown in upper panel of Figure 4 (Sasikumar Raja et al. 2016). Further, assuming the kinetic Alfvén wave dispersion equation we derived the heating rate.

3.4. Solar wind heating rate

In this paper, we used the density modulation indices (ϵ_{N_e}) derived using the above method (see §3.3) to measure the heating rates. Following Chandran et al. (2009a); Sasikumar Raja et al. (2017), we assume that density fluctuations at small scales are manifestations of low frequency, oblique ($k_{\perp} \gg k_{\parallel}$), Alfvén wave turbulence and are often referred to kinetic Alfvén waves. Here, the quantities k_{\perp} and k_{\parallel} are the components of the wave vector k in perpendicular and parallel direction to the background large-scale magnetic field, respectively.

As previously discussed we envisage a situation where the “balanced” counter propagating Alfvén waves (i.e. with zero helicity) cascade and resonantly damps on the protons at the inner scale and thereby heats the solar wind. Because of the passive mixing of the Alfvén waves with other modes at the inner scale our proton heating rate measurements provide an upper limit. The proton heating rate (i.e. the turbulent energy cascade rate) at inner scales is (Hollweg 1999; Chandran et al. 2009a; Ingale 2015b),

$$\epsilon_{k_i}(R) = c_0 \rho_p k_i(R) \delta v_{k_i}^3(R) \text{ erg cm}^{-3} \text{ s}^{-1}, \quad (14)$$

where, $\rho_p = m_p N_e(R)$ g cm⁻³ with m_p is the proton mass [in grams], $k_i = 2\pi/l_i$ and δv_{k_i} are the wavenumber and magnitude of turbulent velocity fluctuations at inner scales, respectively.

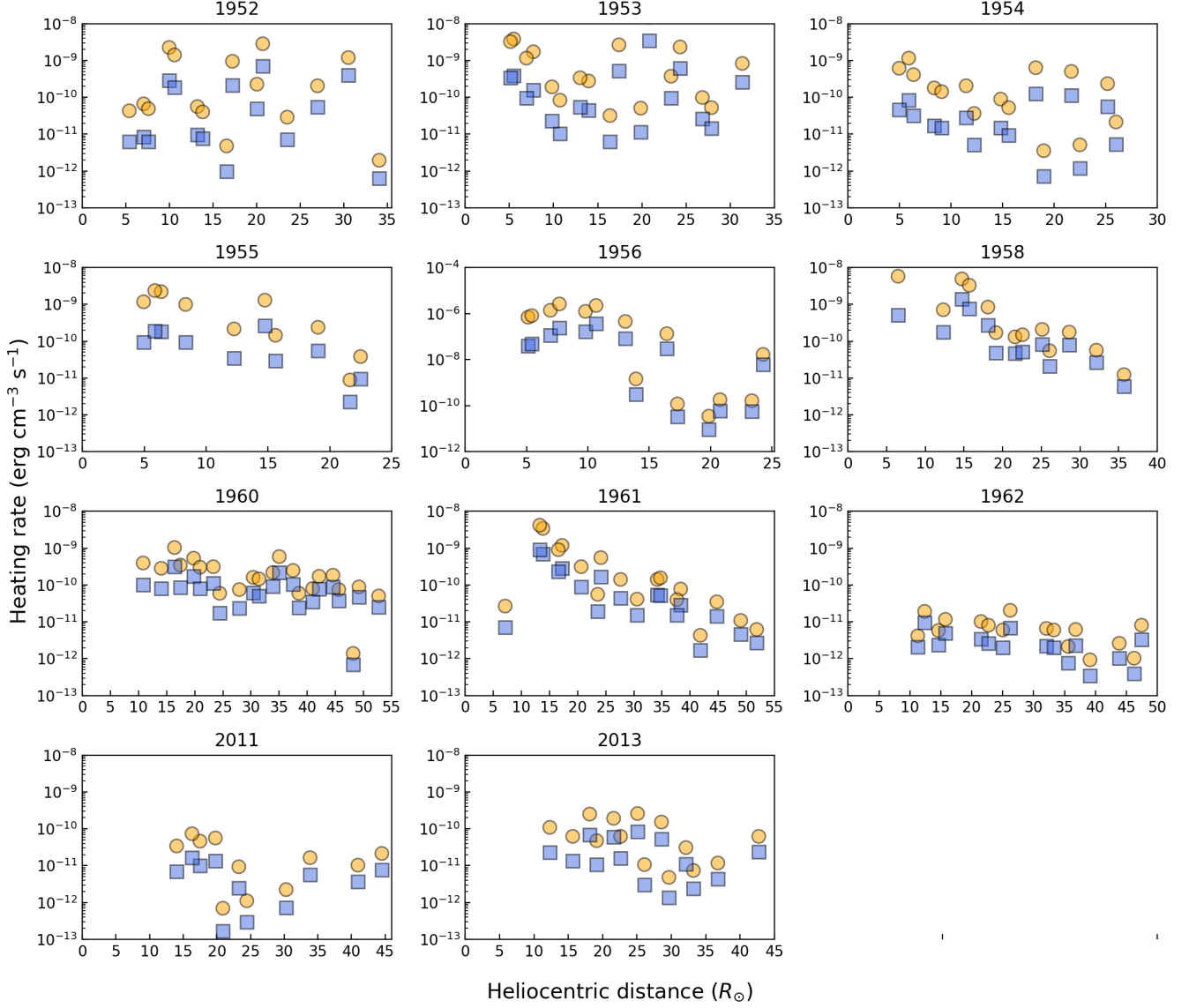


Figure 3. Heliocentric dependence of the proton heating rate in different years. The markers ‘circle’ and ‘square’ indicate proton heating rates that are derived using the proton inertial length and proton gyroradius model, respectively.

The dimensional less quantity c_0 is assumed to be 0.25 (Howes et al. 2008; Chandran et al. 2009a; Sasikumar Raja et al. 2017).

By knowing the ϵ_{N_e} , we calculated δv_{k_i} using the kinetic Alfvén wave dispersion relation (Howes et al. 2008; Chandran et al. 2009a; Ingale 2015b; Sasikumar Raja et al. 2017)

$$\delta v_{k_i}(R) = \left(\frac{1 + \gamma_i k_i^2(R) \rho_i^2(R)}{k_i(R) l_i(R)} \right) \epsilon_{N_e}(R, k_i) v_A(R). \quad (15)$$

where, the adiabatic index γ_i is taken to be 1 (Chandran et al. 2009a; Sasikumar Raja et al. 2017). The Alfvén speed (v_A) in the solar wind is measured using,

$$v_A(R) = 2.18 \times 10^{11} \mu^{-1/2} N_e^{-1/2}(R) B(R) \text{ cm s}^{-1}, \quad (16)$$

The magnetic field strength (B) is estimated using the Parker spiral magnetic field in the ecliptic plane using (Williams 1995),

$$B(R) = 3.4 \times 10^{-5} R^{-2} (1 + R^2)^{1/2} \text{ Gauss}, \quad (17)$$

where, ‘R’ is the heliocentric distance in units of AU.

The derived proton heating rates in different years are shown in Figure 3 and we found that heating rates vary from $\approx 1.58 \times 10^{-14}$ to 1.01×10^{-8} erg cm $^{-3}$ s $^{-1}$ over the heliocentric distances 5 - 45 R_\odot . The markers ‘circle’ and ‘square’ indicate proton heating rates derived assuming different inner scale models - proton inertial length and proton gyroradius model. For latter case, the inner scales are measured using the proton temperature derived using equations 9 and 10.

At 5 R_\odot , in the coronal holes (i.e., in the fast solar wind), the estimated proton heating rates range from 2×10^{-10} and 1.4×10^{-8} erg cm $^{-3}$ s $^{-1}$ (Chandran et al. 2009a). Similarly, at 1 AU the estimated heating rate is 5×10^{-16} erg cm $^{-3}$ s $^{-1}$ (Chandran et al. 2009a). The heating rates derived assuming density fluctuations are due to the kinetic Alfvén waves in the heliocentric distance range 2-174 R_\odot using interplanetary scintillation (IPS) observations (Hewish & Wyndham 1963; Manoharan et al. 2000; Janardhan et al. 2011; Sasikumar Raja et al. 2019b) are 3×10^{-8} erg cm $^{-3}$ s $^{-1}$ (during solar maximum) and $\approx 10^{-15}$ erg cm $^{-3}$ s $^{-1}$ (during solar minimum) consistent with our estimates (Ingale 2015b). Using two-dimensional imaging angular broadening observations of Crab Nebula, the measured heating rates are varied from 2.2×10^{-13} to 1.0×10^{-11} erg cm $^{-3}$ s $^{-1}$ in the projected heliocentric distance range 9 – 20 R_\odot (Sasikumar Raja et al. 2017). The recently reported heating rates in the

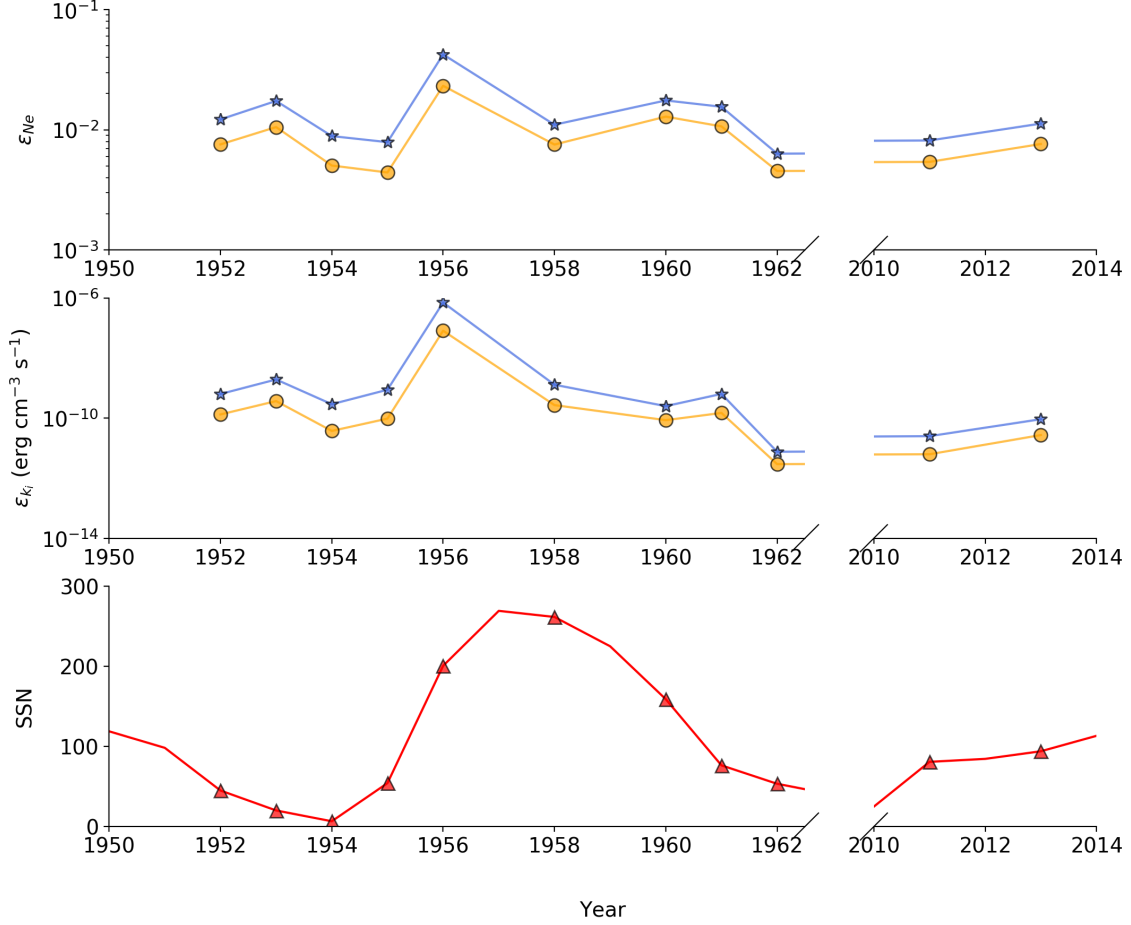


Figure 4. (top) Solar cycle dependence of the modulation index averaged over the heliocentric distance $5 - 45 R_{\odot}$. (middle) Solar cycle dependence of the proton heating rate averaged over the heliocentric distance $5 - 45 R_{\odot}$. The measurements for various inner scale models, i.e., proton inertial length and proton gyroradius models are indicated with the symbols ‘circle’ and ‘square’, respectively. (bottom) The solid line shows the yearly averaged sunspot number (Clette et al. 2016) and the symbol ‘triangle’ indicates the sunspot number in which we have the radio observations. The Figure shows a clear solar cycle dependence of the proton heating rate.

heliocentric distance range $1.5 - 4.0 R_{\odot}$ varied from $\approx 3.31 \times 10^{-10}$ to 4.5×10^{-7} erg cm $^{-3}$ s $^{-1}$ (Cranmer 2020). Further, the author extrapolated these heating rates to the distances 0.3-0.6 AU and it range from $\approx 10^{-15}$ to 10^{-14} erg cm $^{-3}$ s $^{-1}$ and at 1 AU, the extrapolated heating rates are few times of 10^{-16} erg cm $^{-3}$ s $^{-1}$.

Using in-situ measurements by Parker Solar Probe, [Bandyopadhyay et al. \(2020\)](#) estimated energy transfer rates of $8.7 \pm 0.3 \times 10^{-13}$ erg cm⁻³ s⁻¹ at $36 R_{\odot}$ and $5.8 \pm 1.3 \times 10^{-14}$ erg cm⁻³ s⁻¹ at $54 R_{\odot}$. They originally have quoted numbers in units of J kg⁻¹ s⁻¹. We have multiplied their numbers by $N_p m_p$ (where N_p is the solar wind density derived using Leblanc model ([Leblanc et al. 1998](#)) and m_p is the proton mass) to arrive at heating rates in units of erg cm⁻³ s⁻¹. By comparison, the proton heating rate at $36 R_{\odot}$ from our results (see [Figure 3](#)) range from $\approx 2.8 \times 10^{-10}$ to $\approx 7.4 \times 10^{-13}$ erg cm⁻³ s⁻¹. Similarly, [Adhikari et al. \(2020\)](#) reported that heating rates due to quasi-2D turbulence in the heliocentric distance $\approx 1.6 - 100 R_{\odot}$ range from 1.06×10^{-4} to 1.73×10^{-14} erg cm⁻³ s⁻¹. Authors also reported that the heating rate due to the nearly in-compressible/slab turbulence in the heliocentric distance $\approx 1.3 - 100 R_{\odot}$ range from 4.24×10^{-7} to 1.11×10^{-14} erg cm⁻³ s⁻¹. A summary of these proton heating rates is given in [Table 1](#).

As the density modulation indices (see [Figure 2](#)) and heating rates (see [Figure 3](#)) are weakly dependent with heliocentric distance, we averaged the observations that are carried out in different years and plotted in [Figure 4](#). The upper and middle panels of [Figure 4](#) are the averaged density modulation indices and proton heating rates for different inner scale models, respectively. The lower panel shows the yearly averaged sunspot number. [Figure 4](#) shows that the derived density modulation indices and heating rates closely follow the solar cycle. During solar maximum, the slow solar wind drives in all the directions and hence [Sasikumar Raja et al. \(2016\)](#) had justified the lower modulation index in 1958 (also refer to upper panel of [Figure 4](#)). Following the lower density modulation indices, heating rates are lower during the solar maximum.

4. SUMMARY AND CONCLUSIONS

In this article, we have used recently reported density modulation indices ϵ_N derived using angular broadening observations of Crab Nebula ([Sasikumar Raja et al. 2016](#)). The authors have studied the way ϵ_N vary with heliocentric distance and solar cycle (see [Figure 2](#) and [4](#)). Using imaging observations of the Crab Nebula observed in 2016 and 2017, the proton heating rate in the solar corona at various heliocentric distances are reported ([Sasikumar Raja et al. 2017](#)). Using these ϵ_N values and the method discussed by [Sasikumar Raja et al. \(2017\)](#), we measured the proton heating

S.No	R (R_{\odot})	Proton heating rate ($\text{erg cm}^{-3} \text{s}^{-1}$)	References
Remote sensing			
1	5 - 45	$1.58 \times 10^{-14} - 1.01 \times 10^{-8}$	Present work
2	5	$2 \times 10^{-10} - 1.4 \times 10^{-8}$	Chandran et al. (2009a)
3	215	5×10^{-16}	Chandran et al. (2009a)
4	2 -174	$3 \times 10^{-8} - 10^{-15}$	Ingale (2015b)
5	9 - 20	$2.2 \times 10^{-13} - 1.0 \times 10^{-11}$	Sasikumar Raja et al. (2017)
6	1.5 - 4.0	$3.31 \times 10^{-10} - 4.5 \times 10^{-7}$	Cranmer (2020)
7	64.5 - 129	$10^{-15} - 10^{-14}$	Cranmer (2020)
8	215	10^{-16}	Cranmer (2020)
In-situ			
9	36	$8.7 \pm 0.3 \times 10^{-13}$	Bandyopadhyay et al. (2020)
10	54	$5.8 \pm 1.3 \times 10^{-14}$	Bandyopadhyay et al. (2020)
11	1.6 - 100	$1.06 \times 10^{-4} - 1.73 \times 10^{-14}$	Adhikari et al. (2020)
12	1.3 - 100	$4.24 \times 10^{-7} - 1.11 \times 10^{-14}$	Adhikari et al. (2020)

Table 1. Summary of proton heating rates in the solar wind

rate in different years. We found that during 1952 and 2013, the measured proton heating rate ranges from $\approx 1.58 \times 10^{-14}$ to $1.01 \times 10^{-8} \text{ erg cm}^{-3} \text{ s}^{-1}$ in the heliocentric distance $5 - 45 R_{\odot}$ as shown in Figure 3. As the density modulation indices and heating rates weakly depend on the heliocentric distance, we averaged the year's entire observations. The upper and middle panels of Figure 4 show the way the density modulation indices and proton heating rate vary in different years. The lower panel shows the yearly averaged sunspot number in the respective years. Hence we conclude that both density modulation indices and proton heating rate in the solar wind correlates with the solar cycle. The in-situ measurements and thus the derived models (for example, electron / proton density, temperature, and magnetic field) using the Parker Solar Probe which has already covered the heliocentric distance range of $25 R_{\odot}$ and planned to reach as close as $9.86 R_{\odot}$ (Fox et al. 2016) plays a significant role in better understanding proton heating rates and thus the solar wind acceleration.

ACKNOWLEDGMENT

KSR acknowledges the financial support from the Centre National d'études Spatiales (CNES), France. KSR acknowledges O. Alexandrova for the useful discussions that helped in improving the manuscript. The sunspot number used in this article is credited to WDC-SILSO, Royal Observatory of Belgium, Brussels. We thank the referee for constructive suggestions and comments that helped in improving the manuscript.

REFERENCES

- Adhikari, L., Zank, G. P., & Zhao, L. L. 2020, *ApJ*, 901, 102
- Anantharamaiah, K. R., Gothoskar, P., & Cornwell, T. J. 1994, *Journal of Astrophysics and Astronomy*, 15, 387
- Armstrong, J. W., Coles, W. A., Rickett, B. J., & Kojima, M. 1990, *The Astrophysical Journal*, 358, 685
- Bale, S. D., Kellogg, P. J., Mozer, F. S., Horbury, T. S., & Reme, H. 2005, *PhRvL*, 94, 215002
- Bandyopadhyay, R., Goldstein, M. L., Maruca, B. A., et al. 2020, *ApJS*, 246, 48
- Bastian, T. S. 1994, *The Astrophysical Journal*, 426, 774
- Bisoi, S. K., Janardhan, P., Ingale, M., et al. 2014, *The Astrophysical Journal*, 795, 69
- Blesing, R. G., & Dennison, P. A. 1972, *Proceedings of the Astronomical Society of Australia*, 2, 84
- Braude, S. Y., Lebedeva, O. M., Megn, A. V., Ryabov, B. P., & Zhouck, I. N. 1970, *Astrophysics Letters*, 5, 129
- Bruno, R., & Trenchi, L. 2014, *ApJL*, 787, L24
- Chandran, B. D. G., & Hollweg, J. V. 2009b, *ApJ*, 707, 1659
- Chandran, B. D. G., Quataert, E., Howes, G. G., Xia, Q., & Pongkitiwanchakul, P. 2009a, *The Astrophysical Journal*, 707, 1668
- Chen, C. H. K., Leung, L., Boldyrev, S., Maruca, B. A., & Bale, S. D. 2014a, *Geophys. Res. Lett.*, 41, 8081
- . 2014b, *Geophysical Research Letters*, 41, 8081
- Clette, F., Lefèvre, L., Cagnotti, M., Cortesi, S., & Bulling, A. 2016, *SoPh*, 291, 2733
- Coles, W. A., & Harmon, J. K. 1989, *The Astrophysical Journal*, 337, 1023
- Cranmer, S. R. 2020, arXiv e-prints, arXiv:2007.13180
- Cranmer, S. R., van Ballegooijen, A. A., & Edgar, R. J. 2007, *ApJS*, 171, 520
- Cranmer, S. R., van Ballegooijen, A. A., & Woolsey, L. N. 2013, *ApJ*, 767, 125

- Dennison, P. A., & Blesing, R. G. 1972, Proceedings of the Astronomical Society of Australia, 2, 86
- Erickson, W. C. 1964, ApJ, 139, 1290
- Fox, N. J., Velli, M. C., Bale, S. D., et al. 2016, SSRv, 204, 7
- Freeman, J. W. 1988, Geophys. Res. Lett., 15, 88
- Gazis, P. R., Barnes, A., Mihalov, J. D., & Lazarus, A. J. 1994, J. Geophys. Res., 99, 6561
- Goldstein, M. L., Wicks, R. T., Perri, S., & Sahraoui, F. 2015, Philosophical Transactions of the Royal Society of London Series A, 373, 20140147
- Harmon, J. K. 1989, J. Geophys. Res., 94, 15399
- Hewish, A. 1957, The Observatory, 77, 151
- . 1958, MNRAS, 118, 534
- Hewish, A., & Wyndham, J. D. 1963, MNRAS, 126, 469
- Hollweg, J. V. 1999, J. Geophys. Res., 104, 14811
- Howes, G. G., Cowley, S. C., Dorland, W., et al. 2008, Journal of Geophysical Research (Space Physics), 113, A05103
- Ingale, M. 2015b, arXiv e-prints, arXiv:1509.07652
- Ingale, M., Subramanian, P., & Cairns, I. 2015a, MNRAS, 447, 3486
- Ishimaru, A. 1978, Wave propagation and scattering in random media. Volume 1 - Single scattering and transport theory, Vol. 1, doi:10.1016/B978-0-12-374701-3.X5001-7
- Janardhan, P., Bisoi, S. K., Ananthkrishnan, S., Tokumaru, M., & Fujiki, K. 2011, Geophysical Research Letters, 38, L20108
- Krupar, V., Maksimovic, M., Kontar, E. P., et al. 2018, ApJ, 857, 82
- Krupar, V., Szabo, A., Maksimovic, M., et al. 2020, ApJS, 246, 57
- Kulsrud, R. M. 2005, Plasma physics for astrophysics
- Leamon, R. J., Matthaeus, W. H., Smith, C. W., et al. 2000, ApJ, 537, 1054
- Leamon, R. J., Smith, C. W., Ness, N. F., & Wong, H. K. 1999, J. Geophys. Res., 104, 22331
- Leblanc, Y., Dulk, G. A., & Bougeret, J.-L. 1998, SoPh, 183, 165
- Machin, K. E., & Smith, F. G. 1952, Nature, 170, 319
- Manoharan, P. K., Kojima, M., Gopalswamy, N., Kondo, T., & Smith, Z. 2000, ApJ, 530, 1061
- Matthaeus, W. H., Zank, G. P., Smith, C. W., & Oughton, S. 1999, PhRvL, 82, 3444
- McLean, D. J., & Labrum, N. R. 1985, Solar radiophysics: Studies of emission from the sun at metre wavelengths
- Mugundhan, V., Hariharan, K., & Ramesh, R. 2017, Solar Physics, 292, 155
- Prokhorov, A. M., Bunkin, F. V., Gochelashvili, K. S., & Shishov, V. I. 1975, IEEE Proceedings, 63, 790
- Ramesh, R. 2011, in Astronomical Society of India Conference Series, Vol. 2, Astronomical Society of India Conference Series
- Ramesh, R. 2014, in Astron. Soc. India Conf. Ser., Vol. 13, Metrewavelength Sky, ed. J. N. Chengalur & Y. Gupta, 19

- Ramesh, R., Kathiravan, C., & Sastry, C. V. 2001, The Astrophysical Journal, Letters, 548, L229
- Ramesh, R., Subramanian, K. R., Sundara Rajan, M. S., & Sastry, C. V. 1998, Solar Phys., 181, 439
- Richardson, J. D., & Smith, C. W. 2003, Geophys. Res. Lett., 30, 1206
- Sahraoui, F., Huang, S. Y., Belmont, G., et al. 2013, The Astrophysical Journal, 777, 15
- Sasikumar Raja, K., Ingale, M., Ramesh, R., et al. 2016, Journal of Geophysical Research (Space Physics), 121, 11605
- Sasikumar Raja, K., Janardhan, P., Bisoi, S. K., et al. 2019b, SoPh, 294, 123
- Sasikumar Raja, K., Subramanian, P., Ingale, M., & Ramesh, R. 2019a, ApJ, 872, 77
- Sasikumar Raja, K., Subramanian, P., Ramesh, R., Vourlidis, A., & Ingale, M. 2017, ApJ, 850, 129
- Sastry, C. V., & Subramanian, K. R. 1974, Ind. J. Radio and Space Phys., 3, 196
- Slee, O. B. 1959, Aust. J. Phys, 12, 134
- Smith, C. W., Mullan, D. J., Ness, N. F., Skoug, R. M., & Steinberg, J. 2001, J. Geophys. Res., 106, 18625
- Spangler, S. R. 2002, The Astrophysical Journal, 576, 997
- Subramanian, K. R. 2000, J. Astrophys. Astron., 21, 421
- Venzmer, M. S., & Bothmer, V. 2018, A&A, 611, A36
- Verdini, A., Velli, M., Matthaeus, W. H., Oughton, S., & Dmitruk, P. 2010, ApJL, 708, L116
- Williams, L. L. 1995, The Astrophysical Journal, 453, 953
- Woolsey, L. N., & Cranmer, S. R. 2014, ApJ, 787, 160
- Yamauchi, Y., Tokumaru, M., Kojima, M., Manoharan, P. K., & Esser, R. 1998, Journal of Geophysical Research (Space Physics), 103, 6571
- Zank, G. P., Adhikari, L., Hunana, P., et al. 2018, ApJ, 854, 32